ACS OMEGA

Open Access

http://pubs.acs.org/journal/acsodf

Article

Structure and Properties of Epoxy Resin/Graphene Oxide Composites Prepared from Silicon Dioxide-Modified Graphene Oxide

Jin An, Yue Zhang, Xiaojun Zhang, Mingpeng He, Jiang Zhou, Jin Zhou, Yan Liu, Xuebing Chen, Yiwen Hu, Xiuduo Song, Jinyao Chen, Tong Wu, Jian Kang,* and Zhihui Xie

Cite This: *ACS Omega* 2024, 9, 17577−17591

Read Online

ACCESS | Metrics & More | Article Recommendations

ABSTRACT: In this study, graphene oxide (GO) was modified via electrostatic interactions and chemical grafting by silica (SiO_2), and two SiO_2@GO hybrids (GO-A and GO-B, respectively) with different structures were obtained and carefully characterized. Results confirmed the successful grafting of SiO_2 onto the GO surface using both strategies. The distribution of SiO_2 particles on the surface of GO-A was denser and more agglomerated, while it was more uniform on the surface of GO-B. Then, epoxy resin (EP)/GO composites were prepared. The curing mechanism of EP/GO composites was studied by differential scanning calorimetry and in situ infrared spectra spectroscopy. Results of tensile tests, hardness tests, dynamic mechanical analysis, and dielectric measurement revealed that EP/GO-B exhibited the highest tensile properties, with a tensile strength of 79 MPa, a 43% increase compared to raw EP. Furthermore, the addition of fillers improved the hardness of EP, and EP/GO-B showed the highest energy storage modulus of 1900 MPa. The inclusion of SiO_2@GO hybrid fillers enhanced the dielectric constant, volume resistivity, and breakdown voltage of EP/GO composites. Among these, EP/GO-B displayed the lowest dielectric loss, relatively good insulation, and relatively high volume resistivity and breakdown voltage. A related mechanism was proposed.

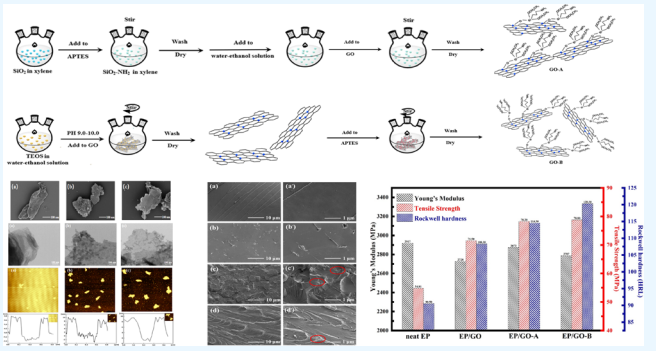

1. INTRODUCTION

Epoxy resin (EP) is a widely used thermosetting resin due to its excellent mechanical properties, chemical stability, insulating properties, and bond strength.[1−4] It serves as the base material for many composites that exhibit an excellent performance. EP finds extensive application in various industrial fields, including electrical equipment insulation materials, high-performance coatings, wind power blade materials, packaging materials, and construction materials.[5−9]

Toughening modification of EP is essential due to issues with their highly cross-linked network structure, including reduced toughness and poor impact resistance, which make it difficult for conventional epoxy resins to meet evolving industrial requirements.[10,11] Various modification methods have been employed, such as rubber toughening modification, organosilicon modification, thermoplastic resin modification, nanofiller modification, etc.[12−15] Among these methods, nanofiller modification has gained significant attention in recent years because inorganic nanoparticles offer excellent toughness and heat resistance. Hybridization of these nanoparticles with EP combines the benefits of both organic and inorganic materials, effectively improving the mechanical properties and thermal stability of polymer materials.[16,17]

Graphene oxide (GO), one of the most commonly used nanofillers, possesses excellent mechanical and thermal conductivity, a huge specific surface area, and a lamellar structure containing abundant oxygen-containing functional groups on the surface and at the edges. These functional groups, such as −COOH, C−O−C, and −OH, provide reactive active sites for chemical grafting.[18,19] However, the enormous specific surface area, $\pi-\pi$ stacking effect, and van der Waals forces of GO make it prone to severe agglomeration in EP and poor dispersion in the matrix as a filler. This can affect the performance of composites.[20,21] Consequently, GO needs to be physically or chemically modified to improve its

Received: January 21, 2024
Revised: March 10, 2024
Accepted: March 15, 2024
Published: April 6, 2024

Scheme 1. Schematic Illustration of the Preparation of the Modified SiO_2@GO Hybrid GO-A by the Electrostatic Adsorption Method and GO-B by the Chemical Grafting Method

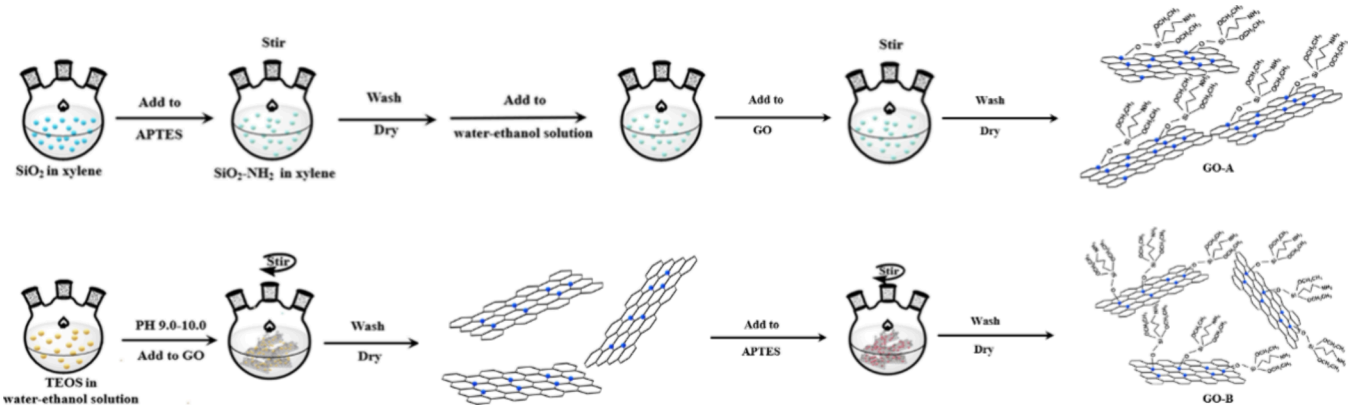

dispersion in the matrix and achieve better interfacial bonding. Nonahal et al.[22] chose amine-capped polyamide amine PAMAM dendrimers to modify GO, resulting in highly curable nanocomposites based on epoxy resin. The modified GO showed improved dispersion in the composites, and the activation energy of the curing reaction was reduced compared to that of the unmodified GO/EP composites. In a similar fashion, Gonçalves et al.[23] employed atom transfer radical polymerization (ATRP) to graft poly(methyl methacrylate) (PMMA) molecular chains onto the surface of GO. This generated chloroform-soluble nanocomposites with good performance at a 1% addition ratio. Additionally, the toughness and thermal stability of the composites improved at this ratio.

Due to its high dielectric strength, high resistivity, and chemical stability,[24] SiO_2 is widely used as a filler in various industrial fields. Modifying GO by SiO_2 can effectively address the issue of easy agglomeration of GO, which improves the composites' comprehensive performance by increasing the number of active sites on the surface of GO.

In recent years, the modification of SiO_2 in GO and the preparation of EP composite have received attention.[25,26] Ramezanzadeh et al.[27] examined the synthesis and characterization of SiO_2 nanofabricated GO (SiO_2-GO) nanohybrids using a two-step in situ sol−gel method. They modified the hybrids with a mixture of 3-aminopropyltriethoxysilane (APTES) and tetraethylsilicate (TEOS). Two facile routes were employed to improve the dispersion properties, barrier properties, and corrosion resistance of the EP coatings by incorporating the hybrids. Ma et al.[28] focused on the depositing of SiO_2 nanohybrids onto GO surfaces using amine-based end-capped hyperbranched polymers (HBPs). The aim was to enhance the dispersion and interfacial interactions between GO and EP. Experimental results showed that SiO_2 functionalized with HBP improved the dispersion of GO in EP through covalent bonds. The resulting GO-SiO_2/EP composites exhibited higher mechanical and thermal properties compared to those of GO/EP or SiO_2/EP composites. Wang et al.[29] synthesized γ-(2,3-glycidoxy) propyltrimethoxysilane (GPTS)-functionalized silica nanoparticles ($GSiO_2$) that were grafted onto lysine-modified graphene oxide (LGO) to create GLGO nanohybridized materials. These hybridized materials were used as nanofillers for a waterborne epoxy resin (WEP) matrix. Experimental data demonstrated that the impedance modulus of the GLGO/WEP coating system, with only 0.1 wt % GLGO added at $|Z|_f$ = 0.01 Hz, was approximately two orders of magnitude higher than that of the pure WEP coating after 40 days of immersion.

To introduce SiO_2 onto the GO surface, SiO_2@GO hybrids are typically prepared by using two forms of bonding interactions: electrostatic interactions or chemical grafting methods. However, the effects of different modification methods on the properties of composites have been less frequently investigated in current studies. As a result, there is a lack of in-depth research on which modification method is the most effective and what mechanisms are responsible for these effects on the properties of composites.

In this paper, to address the problems mentioned above, SiO_2@GO hybrids (GO-A and GO-B) were prepared by electrostatic interactions and chemical grafting, respectively. The structural compositions and morphologies of the two SiO_2@GO nanoparticles were finely characterized. Next, EP/SiO_2@GO composites were prepared. A comparative study was conducted on their curing behaviors, mechanical properties, and dielectric properties to reveal the structural differences yielded by the different preparation methods of SiO_2-modified GO. Additionally, the mechanism of action of these effects on the macroscopic properties of EP/SiO_2 @GO composites was discussed and proposed.

2. EXPERIMENTAL SECTION

2.1. Raw Materials. Bisphenol A epoxy resin (industrially pure, E51 grade, epoxy equivalent 184∼195 g/mol) was purchased from Deyuan Chemical Co., Ltd. in China; GO (average particle size 191.10 nm) was purchased from Deyang Encarbon Science and Technology Co. Ltd., China; hydrophilic fumed silica (SiO_2, Hydrophilic-150, specific surface area 150 m^2/g, particle size 7∼40 nm, 99.8%) was purchased from Shanghai Aladdin Biochemical Science and Technology Co, China.

Ammonia ($NH_3 \cdot H_2O$), tetraethoxysilane (TEOS, SiO_2 content ≥28.4%, density 0.932∼0.936 g/mL), xylene, ethanol (CH_3CH_2OH) were analytically pure.

2.2. Sample Preparation. To examine the impact of different SiO_2 modification methods on the properties of EP systems, GO-A and GO-B were synthesized using electrostatic interaction and chemical grafting techniques, respectively. The complete preparation process is illustrated in Scheme 1.

2.2.1. Preparation of GO-A by the Electrostatic Adsorption Method. The specific preparation process of GO-A was as follows: The SiO_2 nanoparticles were first placed in a vacuum

https://doi.org/10.1021/acsomega.4c00707
ACS Omega 2024, 9, 17577−17591

oven at 120 °C for 24 h to remove the absorbed water on their surface. Subsequently, 3 g of SiO_2 and 5 mg of APTES were added into a three-neck flask containing 400 mL of xylene, which was placed in an oil bath at 120 °C and stirred for 5 h. The resulting mixture was washed three times with xylene, filtered, and subsequently placed in a vacuum oven under vacuum conditions at 120 °C for 24 h to eliminate any remaining xylene. Next, in a beaker, modified SiO_2, 0.2 g of GO, 600 mL of ethanol, and 150 mL of H_2O were added and mechanically stirred at room temperature for 12 h. The resulting mixture was then filtered and placed in a vacuum oven at 90 °C for 24 h to remove any remaining ethanol. The final product of this process was named GO-A. The complete preparation process is illustrated in Scheme 1.

2.2.2. Preparation of GO-B by the Chemical Grafting Method. The specific preparation process is shown in Scheme 1. In a beaker, 0.2 g of GO was added along with 600 mL of ethanol and 150 mL of H_2O. The solution was sonicated at room temperature for 1 h. Drops of ammonia solution were then added to adjust the pH of the solution to 9.0−10.0. Next, 10 mL of TEOS was added to the solution, and the resulting mixture was sonicated at room temperature for 12 h. After that, the mixture was centrifuged at 5000 rpm and washed with ethanol three times. In a flask, 5 mg of APTES was mixed with 600 mL of ethanol and 150 mL of H_2O and placed in an oil bath at 50 °C with magnetic stirring for 5 h. The resulting mixture was washed with ethanol three times and then filtered. It was then placed in a vacuum oven under vacuum conditions at 90 °C for 24 h to remove any remaining ethanol. The drying process resulted in the formation of the product, which was named GO-B.

The synthesized SiO_2@GO hybrids were sieved (100 μm) and stored in a vacuum oven at 120 °C for 24 h before use.

2.2.3. Preparation of EP/GO Composites. In a beaker, 0.02 g of GO (raw GO, GO-A, and GO-B) was added, followed by 400 mL of ethanol. The mixture was then sonicated at room temperature for 2 h. Next, 4 g of EP was introduced into the beaker, and the entire system was sonicated again at room temperature for 2 h. Afterward, the system was stirred at 90 °C for 12 h to facilitate the evaporation of the ethanol. Subsequently, the system was placed in a vacuum oven under vacuum conditions at 90 °C for 2 h to ensure the complete removal of any residual ethanol. The final step involved adding JH-0422 amine curing agent, with a mass fraction of 20%, into the system, which was then vigorously stirred until a homogeneous mixture was achieved. The resulting samples of EP/GO, EP/GO-A, and EP/GO-B were obtained by using the earlier preparation.

2.3. Characterization. *2.3.1. Fourier Transform Infrared Spectroscopy (FT-IR).* The spectra of GO, GO-A, and GO-B were recorded in transmission mode by using a Fourier transform infrared spectrometer (FT-IR, PerkinElmer Frontier, PerkinElmer Corp, USA). The scanning range was 4000−400 cm^{-1}, with an accuracy of 4 cm^{-1} and 16 scans.[30,31]

2.3.2. X-ray Photoelectron Spectroscopy (XPS) Analysis. The X-ray photoelectron spectroscopy (XPS, Thermo Scientific K-Alpha, Thermofisher, USA) was used to analyze the chemical structure and composition of the surface of GO, GO-A, and GO-B samples. The experimental conditions included a vacuum of 5×10^{-9} mbar, a monochromatic Alka source (Mono Alka) with an energy of 1486.6 eV, a voltage of 15 kV, a beam current of 15 mA, a CAE analyzer scanning mode, and an instrumental work function of 4.2.[32,33]

2.3.3. Transmission Electron Microscopy (TEM) Analysis. Transmission electron microscopy (TEM, Tecnai G2 F20 S-TWIN, FEI, USA) was performed at an accelerating voltage of 200 kV to further analyze the structure and dimensions of GO-A and GO-B. For this purpose, the TEM samples were dispersed in ethanol and deposited on a copper gate for observation.

2.3.4. X-ray Diffraction Analysis (XRD). The diffractometer (Ultima IV, Rigaku Corp., Japan) was used to obtain the X-ray diffraction (XRD) patterns of GO, GO-A, and GO-B. *Cu* K_α radiation with a wavelength of λ = 0.154 nm was emitted, and the scanning speed was set to 10° /min. Powder samples were used for pure GO, and its spectra were recorded in the range of $2\theta = 0 \sim 90°$.[34−37]

2.3.5. Raman Spectroscopy. The molecular structure of GO was analyzed by using an FT-Raman spectrometer (FTIR-Raman, Renishaw inVia, Bruker Corp., England) with a laser wavelength of 514 nm.

2.3.6. Thermal Weight Loss Analysis (TGA). The oxygen-containing functional group content of raw GO, GO-A, and GO-B was analyzed using thermogravimetric analysis (TGA) with an FG 209 F1 instrument from Netzsch Corp., Germany. A crucible was used to contain approximately 2 mg of the GO powder. The analysis was conducted under a nitrogen (N_2) atmosphere, with a temperature increase rate of 10 °C/min. The temperature range for the analysis was set from 30 to 800 °C.

2.3.7. Differential Scanning Calorimetry (DSC). The standard procedure for each experiment using a differential scanning calorimeter (DSC, DSC1, Mettler Toledo, Switzerland) at a continuous nitrogen flow rate of 50 mL/min was as follows: 5−8 mg of the specimen was taken and heated to 300 °C at a ramp rate of 10 °C/min to analyze the curing behavior.[38−41]

2.3.8. In Situ Infrared Testing. The infrared spectra were collected over a time period of 210 min. An appropriate amount of samples (raw EP, EP/GO, EP/GO-A and EP/GO-B) was uniformly and thinly coated on a pressed potassium bromide sheet. The coated sheet was then placed in an in situ infrared heating attachment. Next, the temperature was increased from 30 to 200 °C at an elevated temperature rate of 10 °C/min. The temperature was maintained at 200 °C for 3 h. The interferences of H_2O and CO_2 were deducted from the scans. The resolution of the IR spectrometer was 4 cm^{-1}, and the scanning range was 400 to 4000 cm^{-1}. The number of scans was 16.

2.3.9. Mechanical Performance Test. The hardness of the casting samples was tested to assess their toughness and resilience. This was done by using a Rockwell hardness tester (TH300, Beijing Time High Technology Co. Ltd., China) specifically designed for samples with a thickness greater than 1 mm and a diameter greater than 3 mm. The tensile properties of both the EP and its composite casting samples were evaluated using a microcomputer-controlled electronic universal testing machine (CMT6104, MTS Systems (China) Co., Ltd., USA). The testing machine was operated at a tensile speed of 10 mm/min to ensure accurate and consistent results.

2.3.10. Scanning Electron Microscopy Analysis (SEM). Scanning electron microscopy (SEM, ZEISS Gemini 300, Carl ZEISS AG, Germany) was employed to observe the fracture surfaces of the pure EP samples and the EP/GO composites after tensile testing at room temperature. To better explore the influence of the microscopic morphology and interfacial

https://doi.org/10.1021/acsomega.4c00707
ACS Omega 2024, 9, 17577−17591

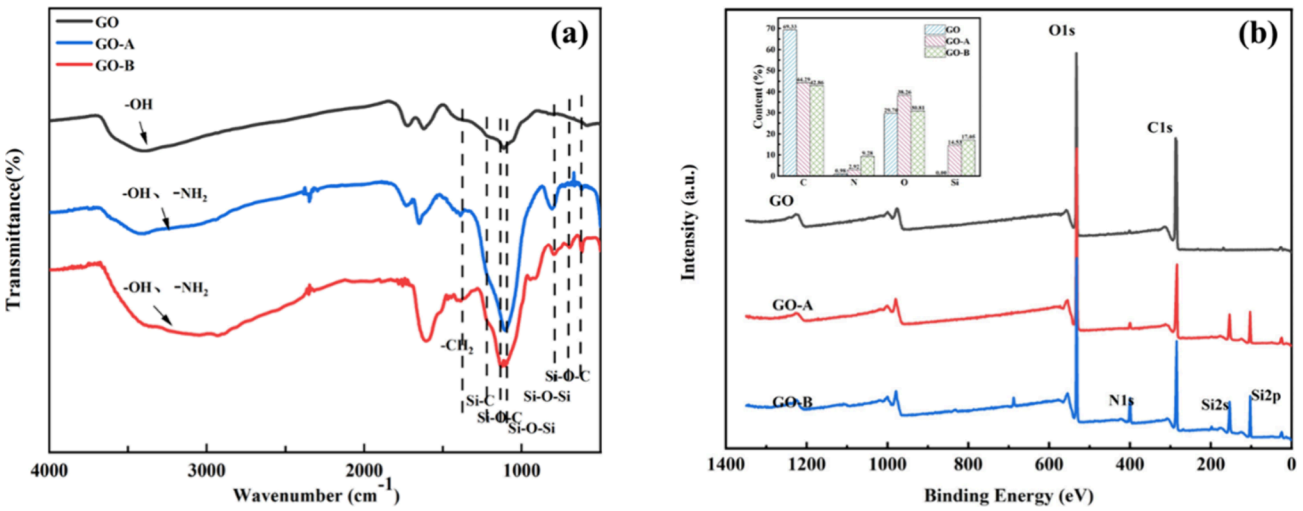

Figure 1. Infrared spectra of raw GO, GO-A, and GO-B (a) and XPS survey spectrum of GO, GO-A, and GO-B (b).

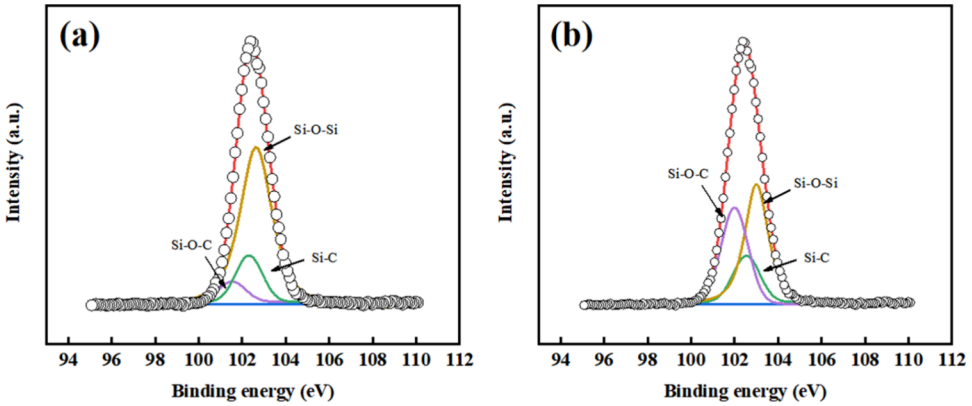

Figure 2. XPS curve fitting of Si_{2p} spectra of GO-A (a) and GO-B (b).

properties of the epoxy nanocomposites on their mechanical properties, the impact fracture surfaces of the samples were coated with gold before the measurements.

2.3.11. Dynamic Mechanical Analysis (DMA). Dynamic mechanical properties of EP and its composite cast samples were tested by using a Dynamic Mechanical Analysis Tester (DMA, Q800, TA Instruments, USA) in a single cantilever beam mode. The test frequency was set at 1 Hz, and the temperature increase rate was set at 3 °C/min. The samples were subjected to a test temperature range of 0 to 120 °C. An applied amplitude of 10 μm was used during testing. The sample size for the tests was 20 × 10 × 4 mm^3.

2.3.12. Dielectric Property Testing. The breakdown voltage of the cast samples was tested using a voltage breakdown tester (DDJ-50 kV, Beijing Guance Instrument Equipment Co. Beijing Guance Instrument Equipment Co., Ltd., China), with a sample thickness of 1 nm and a diameter of more than 20 mm (DC). The dielectric constant and dielectric loss of the samples were measured at room temperature using a broadband dielectric impedance relaxation spectrometer (Concept 50, Novocontrol GmbH, Germany) in the frequency range of 10^1~10^5 Hz, with a sample size of 25 × 25 × 4 mm^3. Additionally, the volume resistance of the cast samples was evaluated by using a high-resistance meter (ZC36, Shanghai Sixth Electric Meter Factory Co. Ltd., China). The sample thickness for this test was more than 0.2 mm, the diameter was more than 55 nm, and the surface was flat.

3. RESULTS AND DISCUSSION

3.1. Structural and Morphological Characterization of SiO_2@GO Hybrids. In this section, FTIR spectroscopy, XPS, TEM, XRD, Raman spectroscopy, and TGA were utilized to characterize the particle size, surface morphology, and chemical structure of raw GO and SiO_2@GO hybrids (GO-A and GO-B, respectively).

The chemical structures of SiO_2@GO hybrids were analyzed by FTIR spectra, as shown in Figure 1a. Among them, the broad peak around 3400 cm^{-1} is the −OH stretching peak, which causes the peak of $-NH_2$ around 3200 cm^{-1} to not be not obvious. Additionally, there are peaks observed around 1230 cm^{-1} for SiO_2@GO hybrids, representing the stretching peak of Si−C. Furthermore, there are peaks around 1130 and 1090 cm^{-1}, resulting from the asymmetric stretching of the −Si−O−C−/−Si−O−Si− bonds. The symmetric telescopic vibrational absorption peaks of the −Si−O−Si− bonds are observed around 800 cm^{-1}, while the symmetric telescopic vibrational absorption peaks of the −Si−O−C−/−Si−O−Si bonds can be seen at around 630 cm^{-1}. Similarly, the peak around 800 cm^{-1} is the symmetric stretching vibrational absorption peak of the −Si−O−Si bond and the peak around 630 cm^{-1} is the vibrational peak of −Si−O−C−. The results in Figure 1a reveal that for GO-A, APTES has been successfully grafted on the surface of SiO_2. The reaction between the modified SiO_2 and the surface of GO takes place, potentially

https://doi.org/10.1021/acsomega.4c00707
ACS Omega 2024, 9, 17577−17591

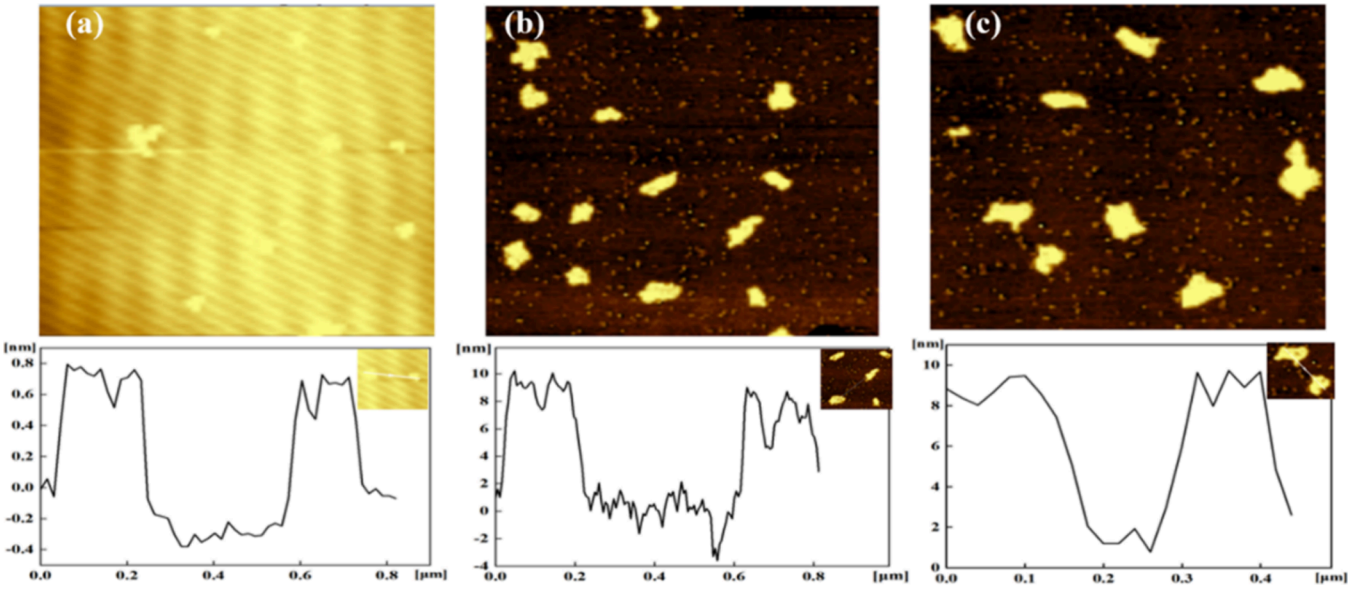

Figure 3. AFM images of the GO (a), GO-A (b), and GO-B (c).

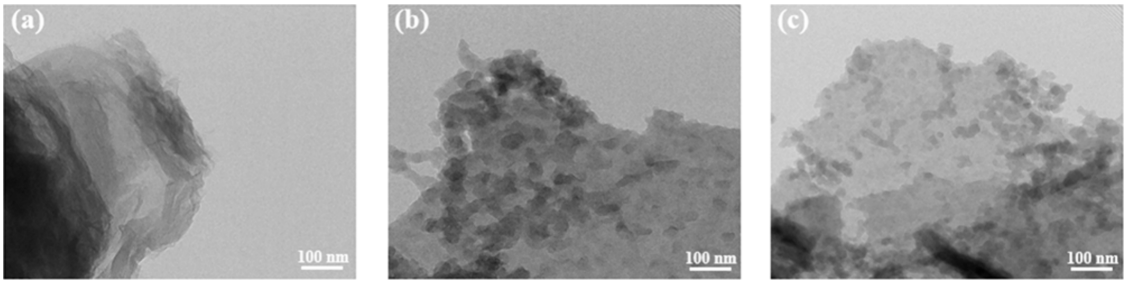

Figure 4. TEM images of GO (a), GO-A (b), and GO-B (c).

due to the presence of $-CH_2$ and $-OH$ on the SiO_2 surface reacting with $-COOH$ and $-OH$ on the GO surface; for GO-B, the FTIR result indicates successful grafting of APTES and hydrolysis and chemical grafting of TEOS onto the GO surface.

The chemical structures and compositions of raw GO and SiO_2@GO hybrid were analyzed by XPS, as shown in Figure 1b, where the major elemental signal peaks of raw GO are those of O_{1s}, C_{1s}, and N_{1s}. In contrast, GO-A and GO-B exhibited elemental signal peaks of O_{1s}, C_{1s}, N_{1s}, Si_{2s}, and Si_{2p}, indicating the successful grafting of SiO_2 onto the GO surface. The relative percentages of C, O, and Si on the surface of GO-A and GO-B are approximately the same as those on the surface of raw GO. The C/O ratios of GO-A and GO-B are 1.16 and 1.39, respectively, while the C/O ratio for raw GO is 2.33. The O/Si ratio of GO-A is 2.63, suggesting the presence of uncondensed $-OH$ and $-COOH$ on its surface alongside SiO_2. On the other hand, GO-B has an O/Si ratio of 1.81, indicating greater silane on the surface of GO. Moreover, the N elemental contents are 2.92% for GO-A and 9.28% for GO-B, demonstrating the improved grafting effect of APTES on GO-B via the chemical grafting method.

The Si_{2p} spectral curves of GO-A and GO-B were fitted, as shown in Figure 2. In the Si_{2p} split-peak spectrum of GO-A, the Si−O−C peak is very weak and almost absent, indicating that the chemical covalent bonding between the modified SiO_2 and GO surface is weak, and it mainly relies on nonchemical covalent bonding. On the other hand, the Si_{2p} spectrum of GO-B can be fitted into three peaks, namely, Si−C, Si−O−C, and Si−O−Si, and the relative intensities of the Si−O−C peaks are larger, while the relative intensities of the Si−O−Si peaks are lower compared with those of GO-A, suggesting that, compared with GO-A, more TEOS have been introduced through hydrolysis to realize chemical grafting on the surface of GO-B.[42]

Moreover, TEM, SEM, and AFM were carried out to analyze the changes in the morphology of GO before and after modification further. The results of AFM in Figure 3 show that most of the raw GO lamellae have a thickness of about 1 nm, indicating its smooth layered structure. However, the SiO_2@GO hybrids of GO-A and GO-B exhibit a thickness of about 10 nm, attributed to the SiO_2 on the GO surface, and the thickness of the SiO_2 overlayer is roughly 9 nm.[43,44]

The TEM images in Figure 4 provide evidence that GO-A and GO-B surfaces are distributed with more uniform and obvious dark spots compared to raw GO. These dense dark spots at the edge folds indicate the higher reactivity of the oxygen-containing functional groups at the GO edges compared to the planar interior, further confirming the successful introduction of SiO_2 on the GO surface of GO-A and GO-B. Among them, GO-A exhibits relatively large dark dots with a diameter of 20−30 nm, some of which show a boundary fusion phenomenon, suggesting agglomeration of SiO_2. On the other hand, GO-B has dark dots with a diameter of about 10−20 nm.

https://doi.org/10.1021/acsomega.4c00707
ACS Omega 2024, 9, 17577−17591

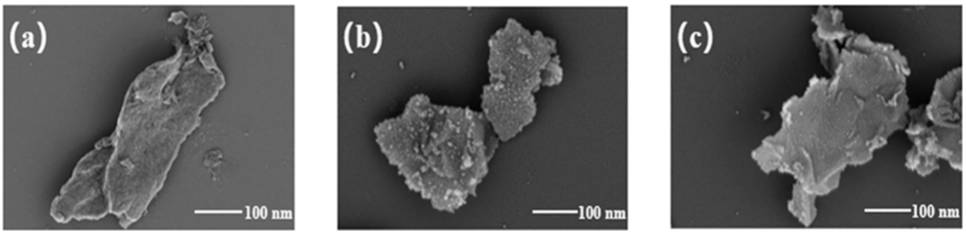

Figure 5. SEM images of the GO (a), GO-A (b), and GO-B (c).

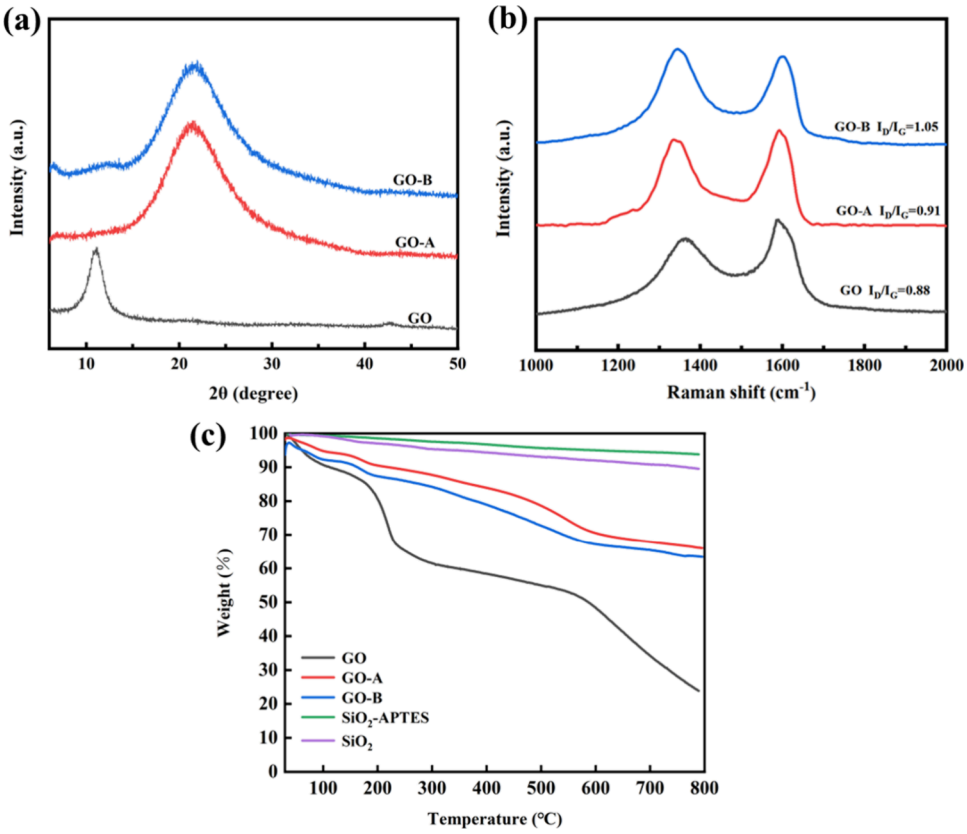

Figure 6. XRD patterns of GO, GO-A, and GO-B (a), Raman spectra of GO, GO-A, and GO-B (b), and TGA curves of GO, GO-A and GO-B (c).

The SEM images in Figure 5 show that the surface of GO is clean, while the modified GO surfaces have fine particles. GO-B has smaller and more uniformly distributed particles, whereas the particles on the surface of GO-A are denser and some appear agglomerated.

Figure 6a displays the XRD patterns of SiO_2@GO hybrids and raw GO. Raw GO exhibits a strong, sharp peak at 2θ = 10°, whereas both GO-A and GO-B show strong, broad peaks at 2θ = 21° due to the dominant effect of SiO_2, attributed to the diffraction of amorphous silicon. Additionally, GO-A has a weak and broad diffraction peak at 2θ = 12°, which is characteristic of GO. Notably, the characteristic peak of GO is not clearly observed in GO-B, implying that the surface of GO-B is densely coated with SiO_2, thereby obscuring its characteristic peak.

The Raman spectra of raw GO and SiO_2@GO hybrids are depicted in Figure 6b. The D peak (1360 cm^{-1}) of GO is attributed to the hybridized portion of sp^3, indicating atomic lattice defects resulting from the vibration of C−C disorder. Additionally, the G peak (1600 cm^{-1}) corresponds to the in-plane vibration of the sp^2 carbon atoms. The I_D/I_G ratio indicates the extent of defects present on the GO surface. Calculation results demonstrate that the I_D/I_G value of the SiO_2@GO hybrids is higher than that of raw GO, indicating increased surface defects. Moreover, the G peak is shifted to the right, signifying the successful introduction of SiO_2 onto the GO surface and consequent structural damage.[45,46] The modified GO layer facilitates efficient peeling. The I_D/I_G values of GO-A and raw GO (0.91 and 0.88, respectively) are quite close, which reveals that the introduction of SiO_2 does not significantly affect the structure in GO-A. Conversely, GO-B displays an I_D/I_G value of 1.05, indicating a noteworthy change compared to the I_D/I_G value of GO. Consequently, it can be concluded that the chemical structure of the GO-B surface has been altered due to successful chemical grafting as TEOS hydrolyzes and chemically interacts with GO, leading to structural destruction.

The TGA curves of the fillers are shown in Figure 6c. It can be observed that SiO_2 exhibits excellent thermal stability, with a residual weight of 93% at 800 °C. On the other hand, SiO_2-APTES modified by APTES grafting shows a decrease in thermal stability, with a residual weight of 89% at 800 °C. This

https://doi.org/10.1021/acsomega.4c00707
ACS Omega 2024, 9, 17577−17591

is attributed to the decomposition of $-NH_2$ under heat, indicating successful grafting and modification of SiO_2.

In contrast, raw GO demonstrates relatively poor thermal stability with three distinct weight loss stages. The initial stage occurs below 100 °C and is attributed to the evaporation of free and bound water. The second stage, around 200 °C, is primarily due to the decomposition and vaporization of oxygen-containing functional groups on GO. Finally, the third stage begins at 500 °C and results from the decomposition of the carbon skeleton of GO. The thermal residual weight of raw GO at 800 °C is calculated to be 25%.

However, the introduction of SiO_2 on the surface of GO to form SiO_2 @GO hybrids significantly enhances their thermal stability. Compared to raw GO, the SiO_2@GO hybrids (GO-A and GO-B) show reduced water loss in the initial stage, indicating a lower hydrophilicity. The second stage of weight loss occurs around 200 °C. It corresponds to the decomposition of physically adsorbed silanes on the surface of SiO_2@GO, as well as the evaporation of products resulting from the self-condensation reactions of these silanes. The third stage of weight loss, starting at 500 °C, is mainly caused by the oxidative thermal decomposition of grafted silanes and the decomposition of the carbon skeleton. The weight loss curve of SiO_2@GO hybrids is smoother, suggesting that nano-SiO_2 particles cover the surface of GO, enhancing thermal stability by inhibiting the decomposition of GO's carbon skeleton and acting as a barrier to heat transfer and gas escape, which is supported by previous studies.[47,48] Furthermore, a comparison between GO-A and GO-B indicates that GO-A exhibits superior thermal stability due to denser and more abundant SiO_2 nanoparticles on its surface, enhancing its heat resistance.[49]

3.2. Curing Mechanism Study. *3.2.1. DSC Test.* The EP/GO composites were characterized by using DSC. Figure 7 displays the DSC curves of enthalpy versus temperature for the EP/GO composites with a heating rate of 10 °C/min.

The overall curing process, as depicted in Figure 7, exhibited that the presence of SiO_2 led to a reduction in the curing temperature of the EP. Specifically, the peak temperature of curing (T_p) of EP/GO-A decreased by approximately 7 °C compared to EP/GO, while the T_p of EP/GO-B decreased by around 15 °C. These findings suggest that the catalytic effects of SiO_2@GO hybrids are more pronounced in the curing process of EP compared to unmodified GO. Furthermore, the catalytic effect of GO-B is superior to that of GO-A.

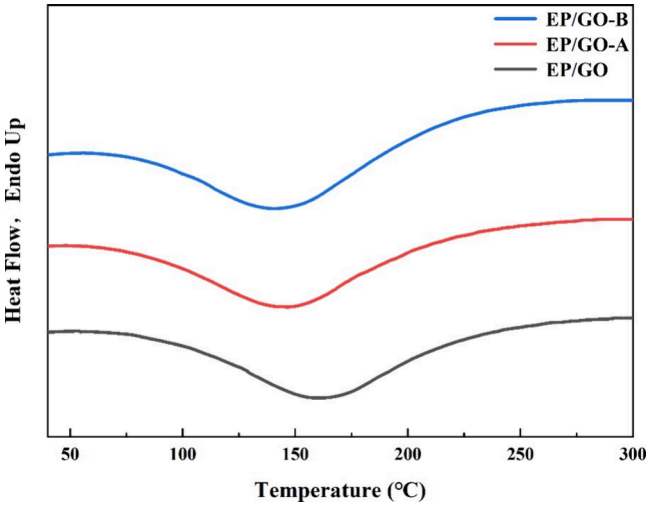

Figure 7. DSC curves of EP/GO, EP/GO-A, and EP/GO-B at 10 °C/min heating rates.

A possible mechanism is proposed: SiO_2 modification introduces more Si−O−H and $-NH_2$ on the surface of GO-A and GO-B compared to unmodified GO. The presence of −OH allows it to react with the C−O−C of EP, resulting in an autocatalytic role.[50] Additionally, the introduction of $-NH_2$ from the grafted APTES acts as an amine-type curing agent, promoting the curing reaction.[51] Furthermore, the SiO_2 layer covering the GO surface serves as a physical intermediate layer between the GO and the EP matrix. This intermediate layer reduces agglomeration, improves dispersion in the matrix, and facilitates the movement of EP molecules during the later stages of the reaction. Comparatively, GO-B exhibits a more uniform distribution of SiO_2 on its surface compared to GO-A, demonstrating SiO_2 agglomeration. After TEOS hydrolysis, the products are grafted onto the surface of GO, increasing the presence of $-NH_2$ and thus enhancing the curing reaction's activity and dispersion in the matrix. Consequently, GO-B can play a superior catalytic role in the curing reaction.

3.2.2. In Situ Infrared Spectra. The curing process of EP/GO composites was monitored using in situ FTIR spectroscopy, which provided the spectrogram of EP/GO during the heating process (Figure 8). The infrared spectra obtained covered the wavelength ranges of 980−890 and 3660−3100 cm^{-1}. Table 1 presents the assignments of specific bands within the 980−890 and 3660−3100 cm^{-1} regions of the spectrum. Figure 8 demonstrates that the absorption peak of −OH, located at around 3585 cm^{-1}, gradually increased as the reaction time increased. Moreover, the absorption peak transitioned from being sharp to becoming broad and diffuse, indicating a significant increase in the content of −OH as the reaction progressed. This suggests that the C−O−C in the sample system gradually reduced until it disappeared during the reaction. Additionally, certain peaks in the infrared spectrum, specifically those around 3454, 3360, and 3220 cm^{-1}, gradually disappeared. These peaks correspond to the N−H peaks of the aromatic amine JH-0422 curing agent and the −OH splitting peaks caused by the polarization-induced effect of $-NH_2$. As the reaction proceeded, the consumption of $-NH_2$ weakened the peak intensity, and the polarization-induced effect gradually diminished, weakening the −OH hetero peaks. Around 20 min, the intensity of these peaks stabilized, indicating that the curing agent played a role in the reaction, and the curing reaction occurred rapidly within this time frame. Moreover, a careful examination of Figure 8 reveals that the relative contents of $-NH_2$ and −OH in the EP/GO composites with added SiO_2@GO hybrids are different during the curing process compared to those in raw EP and EP/GO composites with added raw GO. The peak intensity of −OH in the raw EP system was weak before curing, but it increased with the addition of GO filler. Furthermore, the $-NH_2$ and −OH contents of the EP/GO composites with added SiO_2@GO hybrids were further increased compared with the other composites.

3.3. Mechanical Properties. The mechanical properties of EP composites were investigated using tensile and hardness tests to further study the effect of SiO_2@GO hybrids produced by different modification methods on the mechanical properties of EP. The mechanical properties of raw EP, EP/GO, EP/

https://doi.org/10.1021/acsomega.4c00707
ACS Omega 2024, 9, 17577−17591

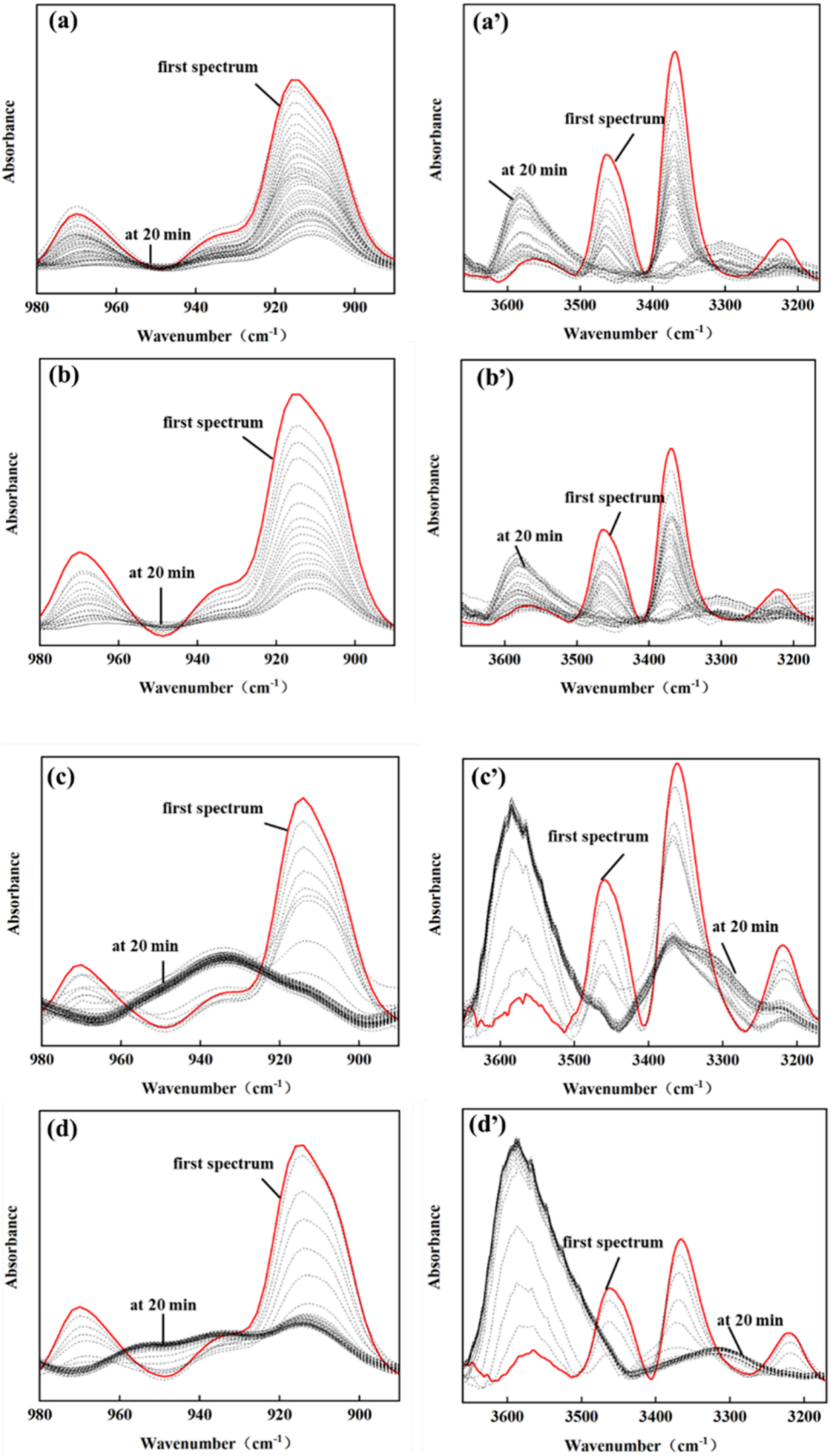

Figure 8. One-dimensional FTIR spectra of raw EP (a), EP/GO (b), EP/GO-A (c), and EP/GO-B (d) collected at 90 s intervals during curing reaction with wavenumber ranges 980−890 and 3660−3100 cm^{-1}.

GO-A, and EP/GO-B were tested, and the results are shown in Figure 9.

The tensile properties of EP/GO composites were significantly improved compared to those of raw EP, as

https://doi.org/10.1021/acsomega.4c00707
ACS Omega 2024, 9, 17577−17591

Table 1. Tentative Assignments of the Spectral Bands in the IR Spectra of Raw EP and EP/GO Composites

band (cm^{-1})	assignment
912	epoxy ring stretching
3228	−OH stretching
3360	−NH stretching
3454	−NH stretching
3585	−OH stretching

shown in Figure 9. Furthermore, the tensile properties of EP/GO composites with added SiO_2@GO hybrids were even better than those of EP/GO composites. Among the different combinations, EP/GO-B showed the highest improvement in tensile strength, increasing by 43% from 55 to 79 MPa compared to raw EP. Additionally, the hardness of the EP/GO composites also demonstrated improvement. Specifically, Young's modulus and hardness of EP/GO composites with added SiO_2@GO hybrids were higher compared to EP/GO composites with added raw GO. The hardness of EP/GO-B was enhanced by 31%, increasing from 91 to 120 HRL compared to raw EP. Although Young's modulus was slightly reduced in EP/GO-B compared to raw EP, the change was minimal.

Both nanofillers, GO and SiO_2@GO hybrids, have improved the mechanical properties of the EP matrix based on the analysis of the mechanical properties of the EP/GO composites described above. This improvement can be attributed to several factors. First, GO possesses a large specific surface area and excellent mechanical properties, with numerous folds on its surface that can form a mechanical interlock with the EP chain segments. Additionally, the surface and edges of GO lamellae contain numerous oxygen-containing groups that react with the EP matrix, thereby enhancing interfacial interactions and stress transfer efficiency and ultimately improving the mechanical properties of EP/GO composites. Second, SiO_2, as a rigid particle, has an intrinsic reinforcing effect, and the presence of SiO_2 in the modified SiO_2@GO hybrids allows for easier peeling off of the hybrids, reducing the agglomeration of GO during composite preparation. As a result, the dispersion of nanofillers in the EP matrix and their compatibility with the EP are improved. Furthermore, the modified SiO_2@GO hybrids possess −OH and $-NH_2$ groups on their surface, which form additional chemical bonds with the EP matrix during the curing process, further enhancing the mechanical properties of the EP/GO composites. It is important to note that the characterization of GO-A and GO-B revealed that the distribution of SiO_2 nanoparticles on the surface of GO-B is relatively finer and more uniform. Additionally, GO-B has chemically grafted silanes on its surface that can react with EP to form a cross-linked network. In contrast, the SiO_2 particles on the surface of GO-A are agglomerated, creating stress concentration points that adversely affect the material's mechanical properties. Consequently, the mechanical properties of EP/GO-B are the most superior among all of the evaluated composites.

To better explore the influence of the microscopic morphology and interfacial properties of the epoxy nanocomposites on their mechanical properties, the fracture surface of the samples after tensile testing at room temperature was observed by scanning electron microscopy (SEM), the results of which are shown in Figure 10. The SEM images with low magnification reveal that the fracture surface of pure EP is smooth, forming obvious smooth and consistent river lines. This observation suggests that the river line structure absorbs part of the fracture energy, and the energy is not impeded in the transfer process. Comparatively, the fracture surface of EP/GO composites exhibits fracture protrusion structures with shorter and more diffuse fracture lines. Notably, the presence of GO lamellar structure at the fracture indicates an improvement in toughness. On the other hand, EP composites with SiO_2@GO hybrids display complex fish scale cracks on the tensile section. These cracks are rougher and accompanied by more tough recessed regions. The formation of these fracture surfaces requires more energy absorption, resulting in an increased toughness and larger fracture energy. Moreover, in Figure 10c,d, a few visible GO lamellae embedded in the EP matrix can be seen on the fracture surface of the samples with SiO_2@GO hybrids. This indicates good interfacial bonding and interaction between the EP and SiO_2@GO hybrids. Furthermore, the better dispersion and adhesion of SiO_2@GO hybrids in the EP matrix compared to GO lead to a transfer of energy from the EP to the filler and can form more microcracks near the particles and divert the cracks, or they hinder the expansion of cracks, resulting in ripples and fish

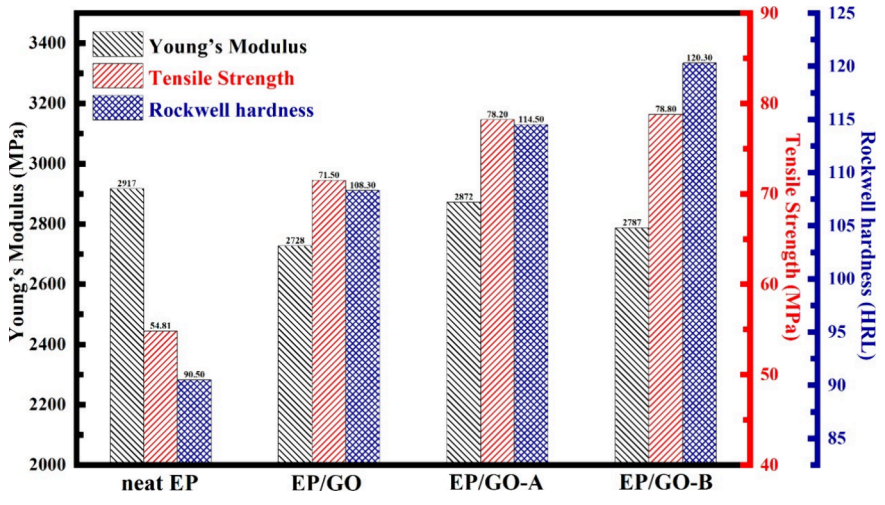

Figure 9. Tensile strength, modulus, and hardness of samples.

https://doi.org/10.1021/acsomega.4c00707
ACS Omega 2024, 9, 17577−17591

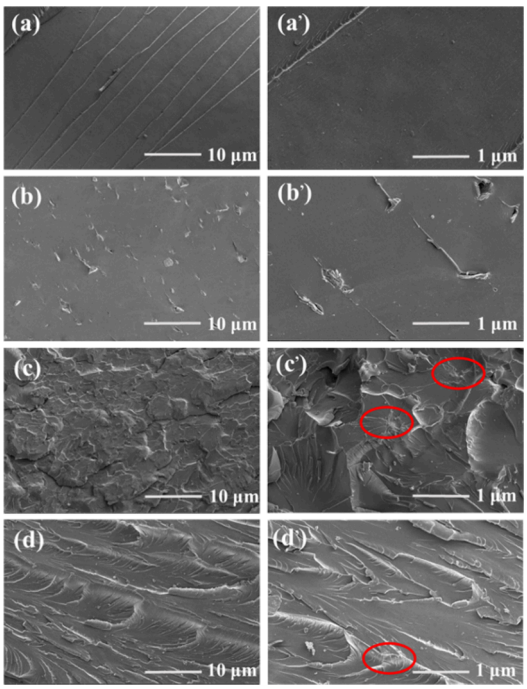

Figure 10. Fractographies of neat EP (a), EP/GO (b), EP/GO-A (c), and EP/GO-B (d) fractured at room temperature.

scale structures in the cross section, thereby improving strength.

3.4. DMA Testing. DMA is an effective means to characterize the viscoelasticity of raw EP and EP/GO composites. The loss factor (tan δ) and energy storage modulus (E') versus temperature curves of raw EP and EP/GO composites are shown in Figure 11. The energy storage modulus of the EP/GO composites was improved to different degrees with the addition of GO nanofillers, which was attributed to the reinforcing effect brought about by the GO lamellae with excellent mechanical properties. Comparing the EP composites with raw GO, it can be found that the energy storage modulus of EP composites with SiO_2@GO hybrids is more obvious. This is mainly due to the improvement of the exfoliation degree of the SiO_2@GO hybrids and their dispersion in the EP matrix, which improves the compatibility of the nanofillers and EP. The SiO_2 nanoparticles, being rigid particles, play a synergistic role with the GO. Additionally, the surface of SiO_2@GO hybrids is rich in $-NH_2$ and $-OH$, which can form more chemical bonds with EP, constitute a cross-linked network, and effectively restrict the movement of EP chain segments around the nanofillers, thus improving the energy storage modulus of EP/GO composites. When comparing the EP composites with added SiO_2@GO hybrids, EP/GO-B exhibits the highest energy storage modulus of 1900 MPa, 58% higher than that of the raw EP system of 1200 MPa. This is related to the superior dispersion ability of GO-B compared to GO-A. GO-B successfully grafted more $-NH_2$ on its surface, and the chemically grafted silanes formed a stronger cross-linking network between the filler and the EP matrix.

The glass transition temperature (T_g) reflects the ability of the polymer chain segments to move as it is the lowest temperature at which they are free to move. The movement of chain segments is affected by the incorporation of fillers in the matrix. In the case of EP/GO composites, the addition of raw GO elevates the T_g, indicating that GO restricts the movement of the chain segments. However, the T_g of EP/GO composites is more significantly elevated when SiO_2@GO hybrid fillers are incorporated. This can be attributed to the introduction of SiO_2 on the surface of GO, which weakens the agglomeration phenomenon of GO and increases its dispersion in the matrix. As a result, the contact surface area of EP chain segments with the SiO_2@GO hybrid increases, limiting the movement of EP chain segments to a greater extent. Moreover, the $-NH_2$ and $-OH$ groups present on the surface of SiO_2@GO hybrids can form chemical bonds with the EP resin, enabling the SiO_2@GO hybrid nanosheets to act as cross-linking points that further inhibit the movement of EP chain segments. Comparing the EP/GO composites with added SiO_2@GO hybrids, it is observed that EP/GO-B exhibits the highest T_g value at 108 °C, which is a notable 23% higher than the T_g value of the raw EP system (88 °C). This discrepancy can be attributed to the partial agglomeration of SiO_2 particles on the surface of GO-A, leading to the weakening of its physical intermediate layer and a greater spatial site resistance effect in the EP matrix. Consequently, the curing reaction process results in increased viscosity of the EP/GO composite system

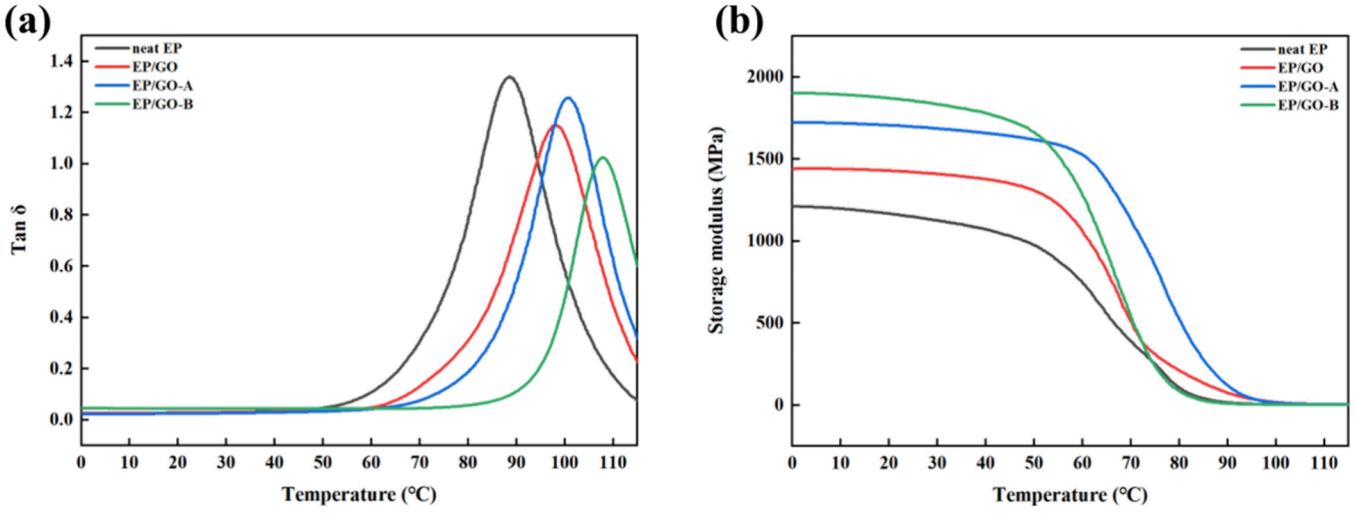

Figure 11. Storage modulus curves (a) and tan δ curves (b) of the raw EP and EP/GO composites.

https://doi.org/10.1021/acsomega.4c00707
ACS Omega 2024, 9, 17577−17591

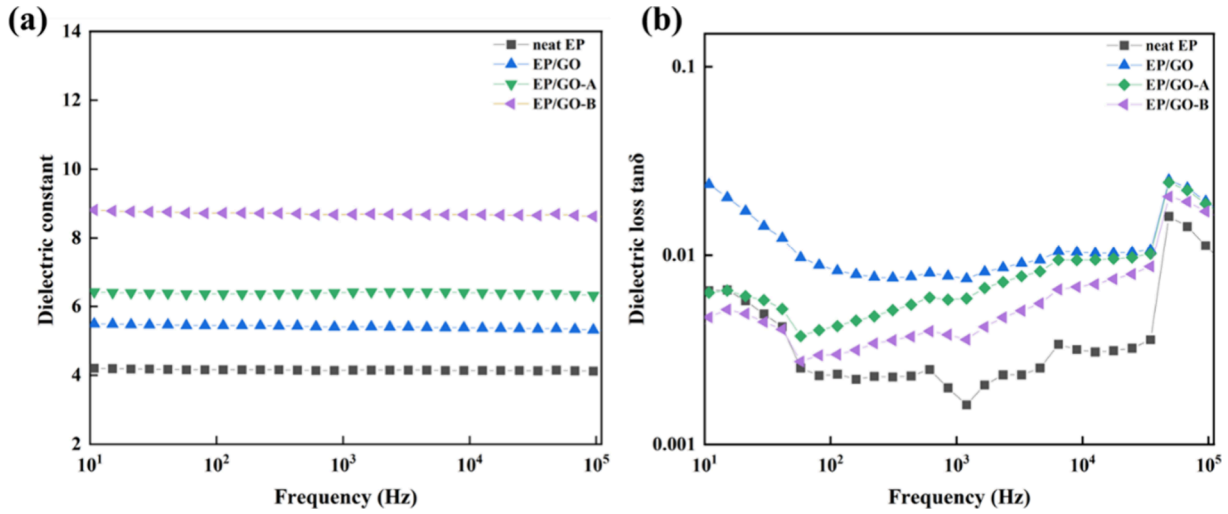

Figure 12. Dependence of dielectric constant (a) and loss on frequency (b) of raw EP and EP/GO composites.

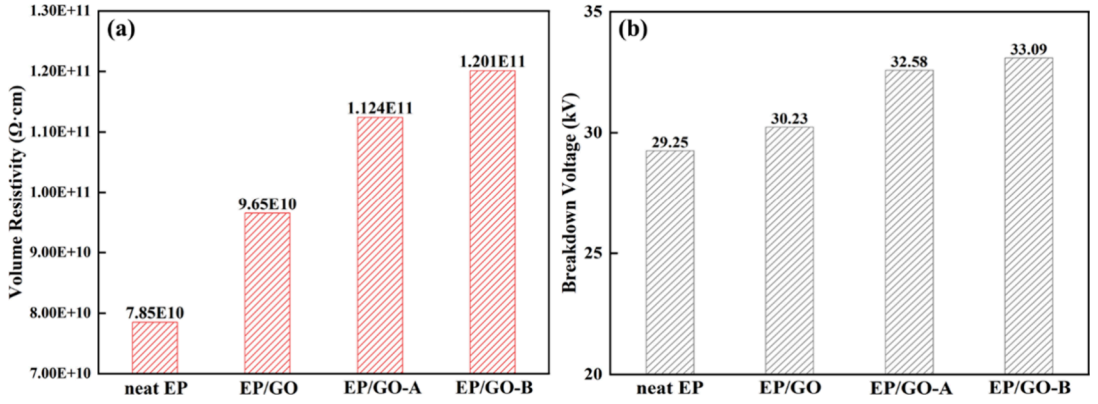

Figure 13. Volume resistivity of samples (a) and breakdown voltage of samples (b).

and the suppression of filler agglomeration, inhibiting the movement of active chains. Consequently, the composites' cross-link density decreases, compromising the curing integrity and ultimately reducing the T_g value.

3.5. Dielectric Property Testing. Figure 12 presents the spectra of the dielectric constant and dielectric loss for the raw EP and EP/GO composites as a function of frequency. The dielectric constants of raw EP and EP/GO composites demonstrate excellent stability within the range of 10^1 to 10^5 Hz, slightly decreasing as the frequency increases. Moreover, the addition of GO nanofillers results in a relative increase in the dielectric constant of the EP system. At the same time, the incorporation of SiO_2@GO hybrid fillers significantly strengthens the dielectric constant of the EP/GO composites. The dielectric constant reflects the ability of a dielectric to store electrostatic energy in an electric field. Due to the organic nature of EP and the inorganic nature of GO, the interface between the two materials produces interfacial polarization and a substantial amount of defects. During electron movement, charge accumulates in these defects, resulting in interfacial polarization and a higher permittivity compared to raw EP. Conversely, after GO modification, the SiO_2@GO hybrids are well-dispersed within the EP matrix, creating an improved charge storage site and consequently leading to a higher dielectric constant.

The dielectric loss of the composites mainly depends on the conductivity loss of the polar impurities as well as the relaxation depletion of the EP polar groups.[52] Raw EP itself has good insulating properties and low conductive loss. However, GO carries polar groups such as −OH, −COOH, etc., and SiO_2@GO hybrids also carry polar groups such as $-NH_2$, −OH, etc., which introduces a certain amount of conductive loss. Furthermore, the functional groups on the surface of GO and SiO_2@GO hybrids react with the functional groups of EP, binding the movement of the polar groups in the EP matrix and thus reducing the relaxation loss of the EP/GO composites.[53] In addition, it can be observed from Figure 12 that the dielectric loss of the material demonstrates a trend of decreasing, then increasing, and then decreasing as the frequency increases. The raw EP without any filler added exhibits the lowest dielectric loss, while EP/GO composites with SiO_2@GO hybrids added have an increased dielectric loss compared to the raw EP but remain below 0.01 overall. Conversely, EP/GO composites with the addition of unmodified GO have a relatively higher dielectric loss compared to that of SiO_2@GO hybrids. The dielectric loss of EP/GO composites is the outcome of the joint influence of conductivity loss and relaxation loss. The EP/GO composites with the addition of SiO_2@GO hybrids demonstrate a higher reduction in relaxation loss compared to the increase in conductivity loss, resulting in lower dielectric loss than EP/GO with the addition of raw GO. Among the EP/GO-A and EP/GO-B composite with SiO_2@GO hybrids added, EP/GO-B exhibits the smallest dielectric loss. This can be attributed to

https://doi.org/10.1021/acsomega.4c00707
ACS Omega 2024, 9, 17577−17591

the fact that GO-A is more susceptible to agglomeration, which leads to a rapid deterioration in the reduction of relaxation loss, resulting in a higher dielectric loss of the composite samples.

The reason the dielectric loss of the material exhibits a pattern of initially decreasing, then increasing, and finally decreasing with the frequency is as follows: as the frequency increases, the polar groups align themselves in response to the electric field, resulting in a decrease in dielectric loss. However, as the frequency increases, the dielectric loss starts to rise, potentially attributed to defects at the two-phase interface. These defects facilitate interfacial polarization, causing electrons to be absorbed into the defects and leading to an increase in dielectric loss. Ultimately, when interfacial polarization reaches its maximum, the dielectric loss decreases again with the frequency.

As shown in Figure 13a, the volume resistivity of raw EP and EP/GO composites can be observed. The resistivity of raw EP is 7.85×10^{10} Ω·cm, as indicated in the figure. However, when GO is added to the EP composites, the volume resistivity slightly increases. This increase can be attributed to the cross-linked network formed by GO, which creates numerous defects due to extensive functionalization. As a consequence, the system has insulating properties. Moreover, introducing of SiO_2 on the surface of GO filler further contributes to an increase in the volume resistivity of EP/GO composites. This can be attributed to the excellent insulating properties of SiO_2 on the surface of GO, resulting in greater intrinsic resistance for the SiO_2@GO hybrids as compared to GO. The EP/GO-B composites exhibit relatively better insulating properties due to the smaller size and more uniform distribution of SiO_2 particles on their surface. On the other hand, the agglomeration of SiO_2 particles on the surface of GO-A leads to a smaller specific surface area, thereby limiting the realization of the insulating properties.

The electrical breakdown of solid media is similar to that in gases because the collision ionization forms an electron collapse and reaches a certain intensity to destroy the lattice structure of the media, which leads to the breakdown. As shown in Figure 13b, the breakdown voltage of raw EP is 29.25 kV under the DC field from 0 to 50 kV, and the breakdown voltages of EP/GO composites are increased on this basis. This is because the distribution of the electric field inside the material changes due to the space charge effect. At a high electric field, the special charge effect makes the electric field of the EP/GO composites homogenized. At the same time, the raw EP undergoes electric field distortion inside the material due to the injection of space charge. As a result, the breakdown voltage of the EP/GO composites is higher than that of the raw EP. In addition, it is found that the breakdown voltage of the composites is further enhanced by the introduction of SiO_2 on the surface of GO through the comparisons on the graphs. This is related to the better dispersion of SiO_2@GO hybrids in the EP matrix compared to GO, and the best dispersed EP/GO-B composite shows the highest breakdown voltage of 33.09 kV, which is 13% higher compared to raw EP.

3.6. Effects of Different Modification Methods on GO and EP/GO Composites. In Section 3.1, we analyzed the surface morphology and chemical structure of SiO_2@GO hybrids through a series of fine characterizations. FTIR spectra show that APTES has been successfully grafted on the surface of GO, and XPS showed that the O/Si ratio of GO-A prepared by electrostatic interaction is higher than that of GO-B prepared by chemical grafting, which indicates that the grafting effect of APTES on GO-B is better. SEM, TEM, and AFM show that the electrostatic interactions cause SiO_2 to agglomerate on the surface of GO. In contrast, the particles on the surface of chemically grafted modified GO are uniformly distributed and have smaller particle sizes. XRD also shows that SiO_2 on the surface of the samples prepared with electrostatic interactions is more numerous and dense and agglomeration occurs. Raman spectroscopy shows that the introduction of SiO_2 on the surface of GO by electrostatic interactions has a significant effect on the surface of GO. The introduction of SiO_2 on the surface of GO has little effect on the surface structure of GO, while chemical grafting destroys the original structure of the GO surface. TGA results show that the thermal stability of GO-A is superior, which also suggests that due to electrostatic interactions covered with denser SiO_2 nanoparticles, it enhances its thermal resistance.

In Sections 3.2−3.5, different experiments were carried out to characterize the effect of different modification methods on the finally obtained EP/GO composites. The DSC results show that SiO_2@GO hybrids have a more effective catalytic effect on the curing process of EP, whereas GO-B obtained through chemical grafting has a better catalytic effect. The results of mechanical property tests indicated that the mechanical properties of EP/GO-B were better, which could be attributed to the more uniform distribution of SiO_2 nanoparticles on the surface of GO-B. DMA showed that the energy storage modulus and T_g of EP/GO-B were higher, which was also attributed to the agglomeration of SiO_2 particles on the surface of GO-A, which reduced the cross-link density of composites and disrupted the curing integrity. Dielectric property tests showed a higher dielectric loss and decreased volume resistivity and breakdown voltage for GO-A.

4. CONCLUSIONS

In this study, SiO_2@GO hybrids GO-A and GO-B were prepared through electrostatic interactions and chemical grafting methods, respectively. Various characterization methods were employed to confirm the successful preparation of the SiO_2@GO hybrids. The characterization results show that the introduction of SiO_2 on the surface of GO through electrostatic interactions does not break its structure but has the potential to produce agglomeration. In contrast, chemical grafting causes changes in the surface structure of GO, which facilitates the interaction of TEOS with GO. The curing behavior and mechanical and dielectric properties of EP composites were examined to assess the modified effects of GO and SiO_2@GO hybrids. DSC, in situ IR, tensile and hardness tests, DMA, and dielectric property tests were conducted for characterization. The experimental results revealed that the EP/GO-B composite system exhibited a greater reduction in the peak curing temperature and showed superior mechanical and dielectric properties. This can be attributed to the nonagglomerated, uniformly dispersed nano-SiO_2 particles with a larger specific surface area present on the surface of GO-B. Additionally, GO-B underwent chemical grafting, resulting in partially chemically grafted silanes on its surface. These silanes facilitated a better reaction with EP, leading to the formation of a cross-linking network that contributed to the overall improvement of the performance of EP composites.

https://doi.org/10.1021/acsomega.4c00707
ACS Omega 2024, 9, 17577−17591

■ ASSOCIATED CONTENT

Data Availability Statement

Data will be made available on request.

■ AUTHOR INFORMATION

Corresponding Author

Jian Kang − *State Key Laboratory of Polymer Materials Engineering, Polymer Research Institute of Sichuan University, Chengdu 610065, China;* orcid.org/0000-0002-3888-2462; Email: jiankang@scu.edu.cn

Authors

Jin An − *State Key Laboratory of Polymer Materials Engineering, Polymer Research Institute of Sichuan University, Chengdu 610065, China*

Yue Zhang − *Dongfang Electric Machinery Co., Ltd., Deyang 618000, China*

Xiaojun Zhang − *Dongfang Electric Machinery Co., Ltd., Deyang 618000, China*

Mingpeng He − *Dongfang Electric Machinery Co., Ltd., Deyang 618000, China*

Jiang Zhou − *Dongfang Electric Machinery Co., Ltd., Deyang 618000, China*

Jin Zhou − *Dongfang Electric Machinery Co., Ltd., Deyang 618000, China*

Yan Liu − *Dongfang Electric Machinery Co., Ltd., Deyang 618000, China*

Xuebing Chen − *State Key Laboratory of Polymer Materials Engineering, Polymer Research Institute of Sichuan University, Chengdu 610065, China*

Yiwen Hu − *Xi'an Modern Chemistry Research Institute, Xi'an 710065, China*

Xiuduo Song − *Xi'an Modern Chemistry Research Institute, Xi'an 710065, China*

Jinyao Chen − *State Key Laboratory of Polymer Materials Engineering, Polymer Research Institute of Sichuan University, Chengdu 610065, China*

Tong Wu − *State Key Laboratory of Polymer Materials Engineering, Polymer Research Institute of Sichuan University, Chengdu 610065, China;* orcid.org/0000-0002-7993-7896

Zhihui Xie − *Dongfang Electric Machinery Co., Ltd., Deyang 618000, China*

Complete contact information is available at: https://pubs.acs.org/10.1021/acsomega.4c00707

Author Contributions

J.A.: conceptualization, methodology, validation, writing (original draft), writing (review and editing); Y.Z.: formal analysis; X.Z.: formal analysis; Jiang Zhou: formal analysis; Jin Zhou: formal analysis; Y.L.: formal analysis; X.C.: formal analysis, investigation, validation; Y.H.: formal analysis; X.S.: formal analysis; J.C.: formal analysis; T.W.: formal analysis; J.K.: resources, writing (review and editing), supervision, funding acquisition; Z.X.: formal analysis.

Notes

The authors declare no competing financial interest.

■ ACKNOWLEDGMENTS

The authors thank financial support from Deyang City Science and Technology Plan Project (2022KCZ155) and the State Key Laboratory of Polymer Materials Engineering (Grant No. SKLPME 2017-3-02). The authors thank Mr. Zhuo Zheng at State Key Laboratory of Polymer Materials Engineering of Sichuan University for the support of characterizations in this study.

■ REFERENCES

(1) Li, J.; Aung, H.-H.; Du, B. Curing regime-modulating insulation performance of anhydride-cured epoxy resin: A review. *Molecules* **2023**, *28* (2), 547.

(2) Jian, R.-K.; Pang, F.-Q.; Lin, Y.-C.; Bai, W.-B. Facile construction of lamellar-like phosphorus-based triazole-zinc complex for high-performance epoxy resins. *J. Colloid Interface Sci.* **2022**, *609*, 513−522.

(3) Giménez, R.; Serrano, B.; San-Miguel, V.; Cabanelas, J.-C. Recent advances in MXene/epoxy composites: trends and prospects. *Polymers* **2022**, *14* (6), 1170.

(4) Dagdag, O.; Bachiri, A.-E.; Hamed, O.; Haldhar, R.; Verma, C.; Ebenso, E.; Gouri, M.-E. Dendrimeric epoxy resins based on hexachlorocyclotriphosphazene as a reactive flame retardant polymeric materials: a review. *J. Inorg. Organomet. P.* **2021**, *31*, 3240−3261.

(5) Mi, X.; Liang, N.; Xu, H.; Wu, J.; Jiang, Y.; Nie, B.; Zhang, D. Toughness and its mechanisms in epoxy resins. *Prog. Mater. Sci.* **2022**, *130*, No. 100977.

(6) Mousavi, S.-R.; Estaji, S.; Paydayesh, A.; Arjmand, M.; Jafari, S.-H.; Nouranian, S.; Khonakdar, H.-A. A review of recent progress in improving the fracture toughness of epoxy-based composites using carbonaceous nanofillers. *Polym. Composite* **2022**, *43* (4), 1871−1886.

(7) Zhao, X.; Long, Y.; Xu, S.; Liu, X.; Chen, L.; Wang, Y.-Z. Recovery of epoxy thermosets and their composites. *Mater. Today* **2023**, *64*, 72 DOI: 10.1016/j.mattod.2022.12.005.

(8) Umer, R.; Li, Y.; Dong, Y.; Haroosh, H.-J.; Liao, K. The effect of graphene oxide (GO) nanoparticles on the processing of epoxy/glass fiber composites using resin infusion. *Int. J. Adv. Manuf. Technol.* **2015**, *81*, 2183−2192.

(9) Liang, X.; Li, X.; Tang, Y.; Zhang, X.; Wei, W.; Liu, X. Hyperbranched epoxy resin-grafted graphene oxide for efficient and all-purpose epoxy resin modification. *J. Colloid Interface Sci.* **2022**, *611*, 105−117.

(10) Dinakaran, K.; Alagar, M.; Kumar, R.-S. Preparation and characterization of bismaleimide/1, 3-dicyanatobenzene modified epoxy intercrosslinked matrices. *Eur. Polym. J.* **2003**, *39* (11), 2225−2233.

(11) Reghunadhan, A.; Datta, J.; Kalarikkal, N.; Haponiuk, J.-T.; Thomas, S. Toughness augmentation by fibrillation and yielding in nanostructured blends with recycled polyurethane as a modifier. *Appl. Surf. Sci.* **2018**, *442*, 403−411.

(12) He, H.; Gao, F. Resin modification on interlaminar shear property of carbon fiber/epoxy/nano-$CaCO_3$ hybrid composites. *Polym. Composite* **2017**, *38* (9), 2035−2042.

(13) Pathak, A.-K.; Borah, M.; Gupta, A.; Yokozeki, T.; Dhakate, S.-R. Improved mechanical properties of carbon fiber/graphene oxide-epoxy hybrid composites. *Compos. Sci. Technol.* **2016**, *135*, 28−38.

(14) Rahman, M.-M.; Zainuddin, S.; Hosur, M.-V.; Robertson, C.-J.; Kumar, A.; Trovillion, J.; Jeelani, S. Effect of NH_2-MWCNTs on crosslink density of epoxy matrix and ILSS properties of e-glass/epoxy composites. *Compos. Struct.* **2013**, *95*, 213−221.

(15) Mąka, H.; Spychaj, T.; Pilawka, R.; Dziedzic, P. Influence of hybrid carbon nanofillers on the cure behavior and properties of epoxy material. *Polimery* **2016**, *61* (3), 181−188.

(16) Zhou, C.; Gu, A.; Liang, G.; Xia, Y. Tough silica-hybridized epoxy resin/anhydride system with good corona resistance and thermal stability for permanent magnet synchronous wind- driven generators through vacuum pressure impregnation. *Ind. Eng. Chem. Res.* **2015**, *54* (28), 7102−7112.

(17) Yu, W.; Sisi, L.; Haiyan, Y.; Jie, L. Progress in the functional modification of graphene/graphene oxide: a review. *RSC Adv.* **2020**, *10* (26), 15328−15345.

(18) Haeri, Z.; Ramezanzadeh, B.; Ramezanzadeh, M. Recent progress on the metal-organic frameworks decorated graphene oxide (MOFs-GO) nano-building application for epoxy coating mechanical-thermal /flame-retardant and anti-corrosion features improvement. *Prog. Org. Coat.* **2022**, *163*, No. 106645.
(19) Najafi-Shoa, S.; Roghani-Mamaqani, H.; Salami-Kalajahi, M. Incorporation of epoxy resin and graphene nanolayers into silica xerogel network: an insight into thermal improvement of resin. *J. Sol-Gel Sci. Technol.* **2016**, *80*, 362−377.
(20) Wang, M.; Ma, L.; Li, B.; Zhang, W.; Zheng, H.; Wu, G.; Huang, Y.; Song, G. One-step generation of silica particles onto graphene oxide sheets for superior mechanical properties of epoxy composite and scale application. *Compos. Commun.* **2020**, *22*, No. 100514.
(21) Wan, Y.-J.; Gong, L.-X.; Tang, L.-C.; Wu, L.-B.; Jiang, J.-X. Mechanical properties of epoxy composites filled with silane-functionalized graphene oxide. *Compos. Part A-Appl. S.* **2014**, *64*, 79−89.
(22) Nonahal, M.; Rastin, H.; Saeb, M.-R.; Sari, M.-G.; Moghadam, M.-H.; Zarrintaj, P.; Ramezanzadeh, B. Epoxy/PAMAM dendrimer-modified graphene oxide nanocomposite coatings: nonisothermal cure kinetics study. *Prog. Org. Coat.* **2018**, *114*, 233−243.
(23) Gonçalves, G.; Marques, P.-A.; Barros-Timmons, A.; Bdkin, I.; Singh, M.-K.; Emami, N.; Grácio, J. Graphene oxide modified with PMMA via ATRP as a reinforcement filler. *J. Mater. Chem.* **2010**, *20* (44), 9927−9934.
(24) Szybowicz, M.; Nowicka, A.-B.; Sądej, M.; Andrzejewska, E.; Drozdowski, M. Morphology of polyacrylate/nanosilica composites as studied by micro-Raman spectroscopy. *J. Mol. Struct.* **2014**, *1070*, 131−136.
(25) Mousavi, A.; Roghani-Mamaqani, H.; Salami-Kalajahi, M.; Shahi, S.; Abdollahi, A. Grafting of silica nanoparticles at the surface of graphene for application in novolac-type phenolic resin hybrid composites. *Mater. Chem. Phys.* **2018**, *216*, 468−475.
(26) Mousavi, A.; Roghani-Mamaqani, H.; Salami-Kalajahi, M.; Shahi, S.; Abdollahi, A. Modification of graphene with silica nanoparticles for use in hybrid network formation from epoxy, novolac, and epoxidized novolac resins by sol-gel method: Investigation of thermal properties. *Express Polym. Lett.* **2018**, *12*, 187−202.
(27) Ramezanzadeh, B.; Haeri, Z.; Ramezanzadeh, M. A facile route of making silica nanoparticles-covered graphene oxide nanohybrids (SiO_2-GO); fabrication of SiO_2-GO/epoxy composite coating with superior barrier and corrosion protection performance. *Chem. Eng. J.* **2016**, *303*, 511−528.
(28) Ma, L.; Song, G.; Zhang, X.; Zhou, S.; Liu, Y.; Zhang, L. Attaching SiO_2 nanoparticles to GO sheets via amino-terminated hyperbranched polymer for epoxy composites: Extraordinary improvement in thermal and mechanical properties. *Eur. Polym. J.* **2021**, *157*, No. 110677.
(29) Wang, S.; Liu, W.; Shi, H.; Zhang, F.; Liu, C.; Liang, L.; Pi, K. Co-modification of nano-silica and lysine on graphene oxide nanosheets to enhance the corrosion resistance of waterborne epoxy coatings in 3.5% NaCl solution. *Polymer* **2021**, *222*, No. 123665.
(30) Liu, T.; Chen, D.; Cao, Y.; Yang, F.; Chen, J.; Kang, J.; Xu, R.; Xiang, M. Construction of a composite microporous polyethylene membrane with enhanced fouling resistance for water treatment. *J. Membr. Sci.* **2021**, *618*, No. 118679.
(31) Wang, J.; Xu, R.; Yang, F.; Kang, J.; Cao, Y.; Xiang, M. Probing influences of support layer on the morphology of polyamide selective layer of thin film composite membrane. *J. Membr. Sci.* **2018**, *556*, 374−383.
(32) Xiong, B.; Chen, R.; Zeng, F.; Kang, J.; Men, Y. Thermal shrinkage and microscopic shutdown mechanism of polypropylene separator for lithium-ion battery: In-situ ultra-small angle X-ray scattering study. *J. Membr. Sci.* **2018**, *545*, 213−220.
(33) Xu, R.; Wang, J.; Chen, D.; Liu, T.; Zheng, Z.; Yang, F.; Chen, J.; Kang, J.; Cao, Y.; Xiang, M. Preparation and performance of a charge-mosaic nanofiltration membrane with novel salt concentration sensitivity for the separation of salts and dyes. *J. Membr. Sci.* **2020**, *595*, No. 117472.
(34) Yu, Y.; Xiong, B.; Zeng, F.; Xu, R.; Yang, F.; Kang, J.; Xiang, M.; Li, L.; Sheng, X.; Hao, Z. Influences of compression on the mechanical behavior and electrochemical performances of separators for lithium ion batteries. *Ind. Eng. Chem. Res.* **2018**, *57* (50), 17142−17151.
(35) Kang, J.; Chen, D.; Xiong, B.; Zheng, N.; Yang, F.; Xiang, M.; Zheng, Z. Facile route for the fabrication of polypropylene separators for lithium-ion batteries with high elongation and strong puncture resistance. *Ind. Eng. Chem. Res.* **2019**, *58* (51), 23135−23142.
(36) Kang, J.; Yang, F.; Chen, J.; Cao, Y.; Xiang, M. Influences of molecular weight on the non-isothermal crystallization and melting behavior of β-nucleated isotactic polypropylene with different melt structures. *Polym. Bull.* **2017**, *74*, 1461−1482.
(37) Zhang, Q.; Peng, H.; Kang, J.; Cao, Y.; Xiang, M. Effects of melt structure on non-isothermal crystallization behavior of isotactic polypropylene nucleated with α/β compounded nucleating agents. *Polym. Eng. Sci.* **2017**, *57* (9), 989−997.
(38) Kang, J.; Chen, J.; Cao, Y.; Li, H. Effects of ultrasound on the conformation and crystallization behavior of isotactic polypropylene and β-isotactic polypropylene. *Polymer* **2010**, *51* (1), 249−256.
(39) Xu, R.; Xu, G.; Wang, J.; Chen, J.; Yang, F.; Kang, J.; Xiang, M. Influence of l-lysine on the permeation and antifouling performance of polyamide thin film composite reverse osmosis membranes. *RSC Adv.* **2018**, *8* (44), 25236−25247.
(40) Kang, J.; Weng, G.; Chen, Z.; Chen, J.; Cao, Y.; Yang, F.; Xiang, M. New understanding in the influence of melt structure and β-nucleating agents on the polymorphic behavior of isotactic polypropylene. *RSC Adv.* **2014**, *4* (56), 29514−29526.
(41) Xu, R.; Wang, J.; Chen, D.; Yang, F.; Kang, J.; Xiang, M.; Li, L.; Sheng, X. Preparation of pH-responsive asymmetric polysulfone ultrafiltration membranes with enhanced anti-fouling properties and performance by incorporating poly (2-ethyl-2-oxazoline) additive. *RSC Adv.* **2018**, *8* (72), 41270−41279.
(42) Liu, Y.; Shi, Y.; Zhang, D.; Li, J.; Huang, G. Preparation and thermal degradation behavior of room temperature vulcanized silicone rubber-g-polyhedral oligomeric silsesquioxanes. *Polymer* **2013**, *54* (22), 6140−6149.
(43) Zhu, C.; Guo, S.; Fang, Y.; Dong, S. Reducing sugar: new functional molecules for the green synthesis of graphene nanosheets. *ACS Nano* **2010**, *4* (4), 2429−2437.
(44) Yang, S.; Feng, X.; Wang, L.; Tang, K.; Maier, J.; Müllen, K. Graphene-based nanosheets with a sandwich structure. *Angew. Chem., Int. Ed.* **2010**, *49* (28), 4795−4799.
(45) Wan, Y.-J.; Gong, L.-X.; Tang, L.-C.; Wu, L.-B.; Jiang, J.-X. Mechanical properties of epoxy composites filled with silane-functionalized graphene oxide. *Compos. Part A-Appl. S.* **2014**, *64*, 79−89.
(46) Yang, H.; Li, F.; Shan, C.; Han, D.; Zhang, Q.; Niu, L.; Ivaska, A. Covalent functionalization of chemically converted graphene sheets via silane and its reinforcement. *J. Mater. Chem.* **2009**, *19* (26), 4632−4638.
(47) Ramezanzadeh, B.; Ahmadi, A.; Mahdavian, M. J. C. S. Enhancement of the corrosion protection performance and cathodic delamination resistance of epoxy coating through treatment of steel substrate by a novel nanometric sol-gel based silane composite film filled with functionalized graphene oxide nanosheets. *Corros. Sci.* **2016**, *109*, 182−205.
(48) Yu, Z.; Lv, L.; Ma, Y.; Di, H.; He, Y. Covalent modification of graphene oxide by metronidazole for reinforced anti-corrosion properties of epoxy coatings. *RSC Adv.* **2016**, *6* (22), 18217−18226.
(49) Wang, R.; Zhuo, D.; Weng, Z.; Wu, L.; Cheng, X.; Zhou, Y.; Wang, J.; Xuan, B. A novel nanosilica/graphene oxide hybrid and its flame retarding epoxy resin with simultaneously improved mechanical, thermal conductivity, and dielectric properties. *J. Mater. Chem. A* **2015**, *3* (18), 9826−9836.
(50) Xie, H.; Liu, B.; Yuan, Z.; Shen, J.; Cheng, R. Cure kinetics of carbon nanotube/tetrafunctional epoxy nanocomposites by isother-

https://doi.org/10.1021/acsomega.4c00707
ACS Omega 2024, 9, 17577−17591

mal differential scanning calorimetry. *J. Polym. Sci., Polym. Phys.* **2004**, *42* (20), 3701−3712.
(51) Rozenberg, B.-A. Kinetics, thermodynamics and mechanism of reactions of epoxy oligomers with amines. *Epoxy Resins Composites II* **2005**, 113−165, DOI: 10.1007/BFb0017916.
(52) Brosseau, C. Generalized effective medium theory and dielectric relaxation in particle-filled polymeric resins. *J. Appl. Phys.* **2002**, *91* (5), 3197−3204.
(53) Wu, Z.; Lin, B.; Fan, J.; Zhao, J.; Zhang, Q.; Li, L. Effect of dielectric relaxation of epoxy resin on dielectric loss of medium-frequency transformer. *IEEE Trans. Dielectr. Electr. Insul.* **2022**, *29* (5), 1651−1658.

https://doi.org/10.1021/acsomega.4c00707
ACS Omega 2024, 9, 17577−17591